A Dynamic Trio: Inertial Oscillation, Deformation Frontogenesis, and the Ekman–Taylor Boundary Layer

VERN OSTDIEK

Department of Physics and Astronomy, Benedictine College, Atchison, Kansas

WILLIAM BLUMEN

Program in Atmospheric and Oceanic Sciences, University of Colorado, Boulder, Colorado

(Manuscript received 17 April 1996, in final form 1 November 1996)

ABSTRACT

Potential temperature and wind profiles obtained during a case of nighttime low-level deformation frontogenesis are examined. The winds in the lowest kilometer over a region in the central United States are shown to be controlled by thermal wind shear in a stable layer above 400 m, in accordance with the Hoskins–Bretherton semigeostrophic frontogenesis model, and by surface-drag-generated shear in the nearly neutral layer below. In this lower layer, the wind profiles are shown to be in good agreement with a simple baroclinic Ekman–Taylor model. The opposite shear in the two layers produces a low-level jet that appears in soundings taken hundreds of kilometers apart. The agreement of the observed profiles with these models is revealed only after a height-dependent inertial oscillation in both layers is removed from the rapidly evolving hourly wind data.

1. Introduction

A case of stretching deformation frontogenesis occurred in a nearly stationary frontal zone during the Stormscale Operational and Research Meteorology–Fronts Experiment Systems Test (STORM-FEST), a field experiment whose primary purpose was the investigation of fronts and related processes in the central United States. The event took place during the night of 20–21 February 1992. A weak cold front moved into the STORM-FEST region during the afternoon of 20 February and then remained nearly stationary for the next 20 h. The position of the wind shift line at 1800 LST[1] and at 0600 LST are shown in Fig. 1. [The locations of the instruments whose data are referred to in this paper are marked as well. The surface map and 500-mb map are shown in Ostdiek and Blumen (1995, hereafter OB; Fig. 3.] Satellite images show partly to mostly cloudy skies throughout the period. No precipitation was reported by any of the surface stations.

Unfortunately, this event did not occur during an intensive observation period. Consequently there were no supplementary soundings or aircraft flights during the 12-h period under consideration. Two of the five National Oceanic and Atmospheric Administration (NOAA) 915-MHz boundary layer profilers (BLP) deployed for STORM-FEST do provide complete hourly averaged wind data, as do the three NOAA demonstration profilers in the region. The data from the latter are of limited usefulness since the lowest measurements are at 500 m above ground. The radio acoustic sounding system data taken by the BLPs during this event are sparse, contradictory, and in some cases unphysical (i.e., showing superadiabatic lapse rates). Consequently they were not used in this investigation.

An earlier analysis of the event by Ostdiek and Blumen (1995) showed that the semigeostrophic frontogenesis model of Hoskins and Bretherton (1972) successfully accounts for the surface evolution of the front during the 5-h period of observed frontogenesis. Analytical and numerical solutions of the semigeostrophic equations initialized at the beginning of the period predict with reasonable accuracy the observed intensification and relative motion of the potential temperature gradient.

However, as pointed out in OB, there are significant discrepancies between the model predictions and the observed vertical profiles of potential temperature and alongfront wind, particularly in the lowest 400 m of the boundary layer. Moreover, the alongfront and cross-front winds aloft change much more rapidly during the night than can be accounted for by the observed frontogenesis, and they do so in a manner suggestive of an

[1] The LST is Central Standard Time, which is 6 h earlier than UTC.

Corresponding author address: William Blumen, PAOS, CB 311, University of Colorado, Boulder, CO 80309.
E-mail: blumen@paradox.colorado.edu

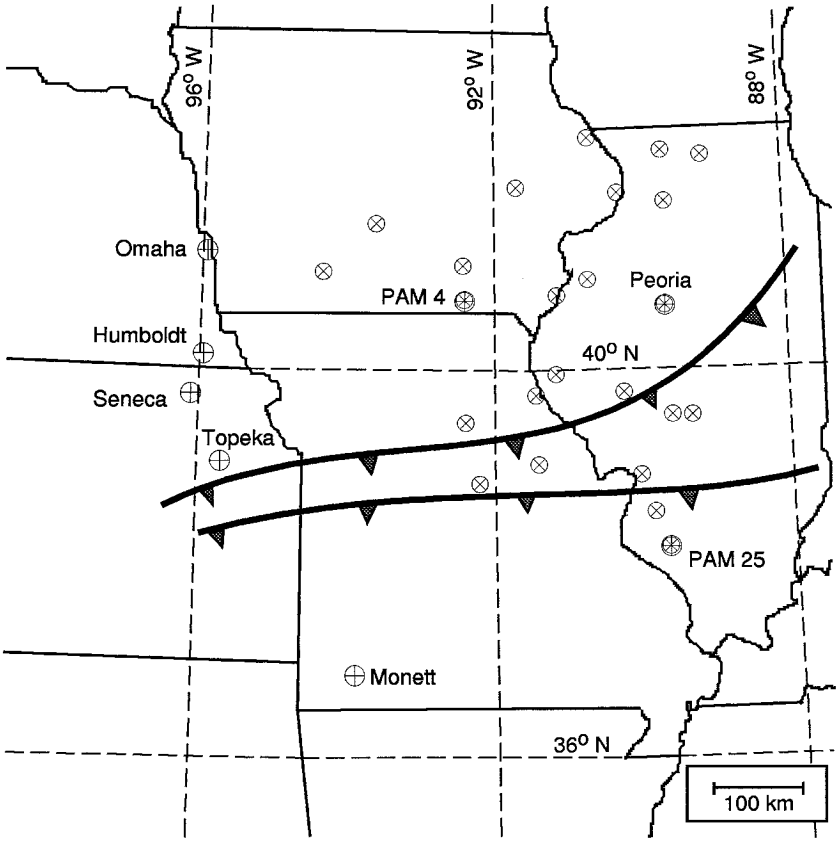

FIG. 1. Map of the central United States showing the southward progression of the wind shift line between 1800 LST (20 February) and 0600 LST (21 February). The locations of specific instruments referred to in this paper are marked by "⊕," and those of surface stations exhibiting inertial oscillation by "⊗" (explained in section 5).

inertial oscillation. It will be demonstrated that the evolution of the wind profiles is also controlled by frictional coupling to the surface in the lower layer, by inviscid semigeostrophic frontogenesis above it, and with a superimposed inertial oscillation in both regions. After filtering this inertial oscillation out of the wind profiles, it is shown that the remaining steady z-dependent part fits a simple baroclinic Ekman–Taylor model in the lower layer and the Hoskins–Bretherton model in the upper layer.

Section 2 is a description of the decomposition of the wind profiles into a steady-state part, which only depends on height z, and an inertial oscillation with height-dependent amplitude and phase. The barotropic–baroclinic boundary layer solution presented by Bannon and Salem (1995) is adopted as a model for the steady-state part of the wind in the nearly neutral lower layer. The root-mean-square fit to the model solutions is shown, in section 3, to be a relatively accurate representation of the data. Section 4 incorporates the boundary layer processes, documented above, into a more comprehensive explanation of front–boundary layer interaction within the context of the semigeostrophic deformation flow model presented by OB. Evidence of inertial oscillations in surface data is described in section 5, along with a discussion of the possible effects on the rate of frontogenesis. A brief description of a similar nocturnal low-level jet, for which there is a more complete set of soundings, is given in section 6, followed by some additional remarks.

2. Vertical profiles and evidence of inertial oscillation

The deformation frontogenesis during the night of 20–21 February took place over a 5-h period (2000 LST–0100 LST). A complete series of upper air wind measurements, from boundary layer profiles located just behind the front, is available. However, there are no collocated temperature data, except at Seneca where one sounding exists. The regular evening and early morning soundings from several sites in and near the frontal zone do provide a partial picture of the vertical profiles that existed 3 h before and then 4 h after the frontogenesis. Figure 2 shows potential temperature, alongfront wind u, and cross-front wind v profiles for five evening soundings. (In some cases, data from collocated surface stations are used because sounding data near the surface

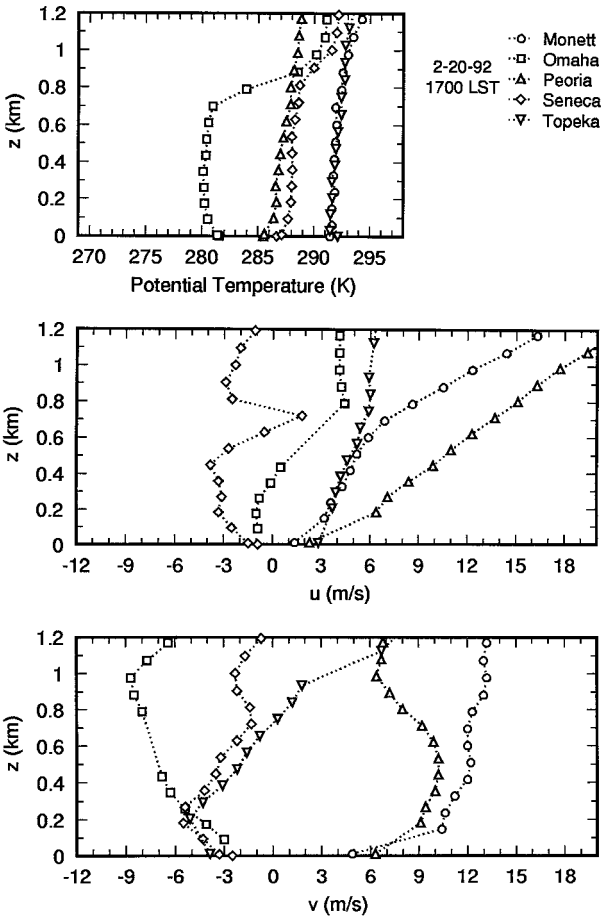

FIG. 2. Vertical profiles of potential temperature, alongfront wind u, and cross-front wind v, taken from available sounding and collocated surface station data at 1700 LST 20 February 1992. Station locations are marked in Fig. 1.

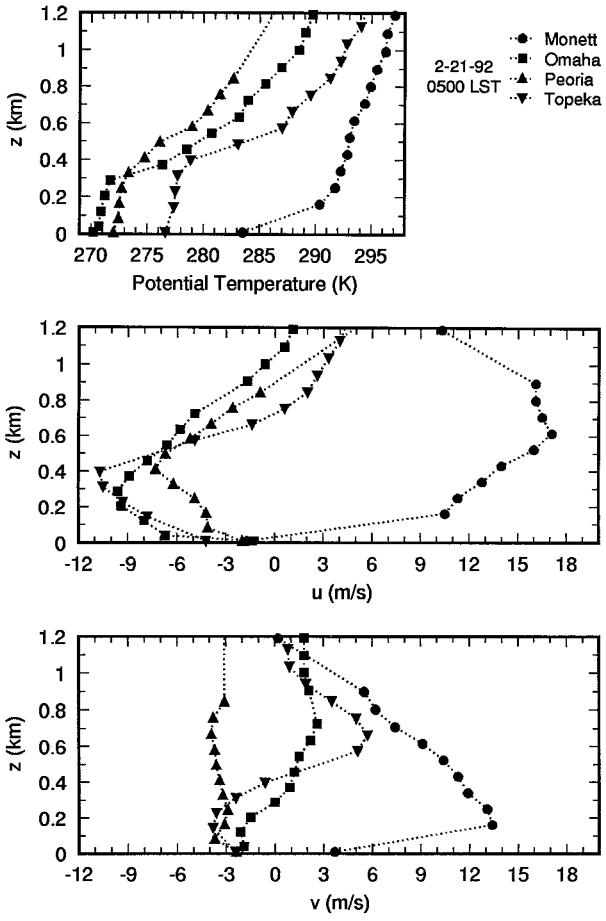

FIG. 3. As in Fig. 2 but for 0500 LST 20 February 1992.

are missing.) Omaha is in the cool northerly flow behind the front, Monett is in the warm air well to the south, and Seneca, Topeka, and Peoria are just to the north of the front. Characteristics of a convective mixed layer are evident in these soundings.

Profiles from four soundings taken the next morning are shown in Fig. 3 (there is no Seneca sounding). The three soundings from behind the front (Omaha, Peoria, and Topeka) are the crucial ones for this investigation. Although these sites are widely separated (250, 530, and 540 km apart), the profiles of potential temperature and alongfront wind are strikingly similar. Each shows a shallow, nearly mixed layer at the surface and an easterly low-level jet. In all three soundings, the height of the low-level jet maximum nearly coincides with that of the base of the overlying thermal inversion. The abrupt change in lapse rate and the reversed shear in alongfront wind, in the lowest 400 m of the atmosphere, are in disagreement with the temperature and wind profile solutions of the Hoskins–Bretherton frontogenesis model.

The evolution of the low-level jet is shown clearly in data from two 915-MHz boundary layer profilers, one collocated with the Seneca sounding site. Figure 4 shows wind profiles at selected times during the night taken by the Seneca profiler. There is good agreement between the wind profiles from the soundings and the corresponding ones from the boundary layer profilers. The large accelerations of the winds throughout the night cannot be accounted for by the modest frontogenesis that takes place.

It should be noted that this alongfront jet is not like the narrow low-level jets ahead of cold fronts, often associated with rain bands, that have been well studied in western Europe (e.g., Kotroni et al. 1994). This low-level jet is behind the front and extends over a wide region.

A simultaneous least-squares fit between the observed u and υ wind at each profiler level and a height-dependent inertial oscillation wind field was performed. In particular, the winds at each level were assumed to evolve according to the representation

$$u(z_i, t_j) = u_{ss}(z_i) + A(z_i)\sin[ft_j + \phi(z_i)],$$
$$\upsilon(z_i, t_j) = \upsilon_{ss}(z_i) + A(z_i)\cos[ft_j + \phi(z_i)], \quad (1)$$

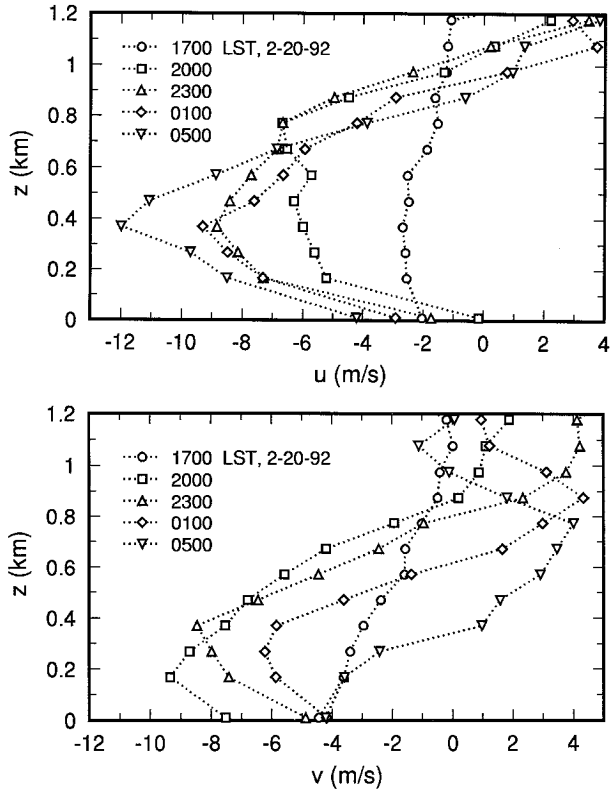

FIG. 4. Observed vertical profiles of hourly averaged alongfront (top) and cross-front (bottom) winds at selected times during the night of 20–21 February 1992, taken by the Seneca boundary layer profiler and collocated PAM station.

where z_i and t_j are the heights and times, respectively, at which the measurements were taken; $u_{ss}(z_i)$ and $v_{ss}(z_i)$ are the height-dependent ''steady-state'' wind speeds; and $A(z_i)$ and $\phi(z_i)$ are the height-dependent amplitude and phase, respectively, of the inertial oscillation. Had the wind profiles initially corresponded to $u_{ss}(z_i)$ and $v_{ss}(z_i)$, they would have remained unchanged through the night. Note that there is no assumption that the basic-state winds are geostrophic, only that they are independent of time. The purpose of this decomposition is to illustrate that inertial oscillations in the winds during the night can account for the large changes in the observed wind profiles.

The wind data, u_{ij} and v_{ij}, from the Seneca boundary layer profiler and the collocated portable automated mesonet (PAM) surface station are hourly averages, taken from t_0 = 1800 LST on 20 February through t_{12} = 0600 LST on 21 February. The levels are z_1 = 11 m (the PAM station), z_2 = 166 m (the lowest profiler level), and z_3 through z_{12} spaced 101 m apart up to 1176 m. The least-squares fit computation consisted of determining the values of $u_{ss}(z_i)$, $v_{ss}(z_i)$, $A(z_i)$, and $\phi(z_i)$ at each level that would minimize the combined root-mean-square (rms) deviation,

$$(\text{rms deviation}_i)^2 = \frac{1}{26}\sum_{j=0}^{12}\left\{[u_{ij} - u(z_i, t_j)]^2 + [v_{ij} - v(z_i, t_j)]^2\right\}, \quad (2)$$

between the measured wind speeds and those given by (1). Note that the amplitude and phase at each level apply to both the u and the v data simultaneously. The Coriolis frequency f ($= 9.3 \times 10^{-5}$ s^{-1}) and the relative phase ($\pi/2$) between the u and the v oscillations are fixed.

As noted earlier in OB, the depth of the deformation flow is approximately 1100 m, and the frontogenesis is confined to this part of the atmosphere. The wind data used in this investigation of inertial oscillation that extends to this altitude might be expected to exhibit behavior indicative of a transition from the boundary layer to the overlying free atmosphere not subject to diurnal effects.

The results of the least-squares fit computation are shown in Figure 5. The combined rms deviation (bottom right) ranges from 0.821 to 1.45 m s^{-1}. The separate contributions of the u and v fits show that most of the deviation is associated with the westerly winds. The fact that the deviations during the 12-h period are roughly 1 m s^{-1}, even though the wind speeds vary over a range as large as 8 m s^{-1}, is noteworthy.

The amplitude of oscillation (Fig. 5, top left) at each height is determined by the differences between the initial and steady-state winds. Here $A(z_i)$ is largest at the height of the jet maximum where this difference is greatest and smallest at the surface. The phase (top right) mainly reflects that initially u is greater than the steady-state value for $z_i < 800$ m and less than it for $z_i > 800$ m. The alongfront steady-state wind profile (bottom left) exhibits a low-level jet, while the cross-front steady-state wind decreases in magnitude monotonically with height up to 1 km, except near the surface.

It is useful to compare the results of the least-squares fit (Fig. 5) to the vertical profile of potential temperature shown in the Topeka sounding taken near the end of the 12-h period (Fig. 3). (Topeka is approximately 95 km south-southeast of Seneca.) The weakly stable layer below ~400 m has strong vertical wind shear and therefore should be coupled to the surface layer by mechanical turbulence. It would be logical to assume that drag would prevent the winds from evolving according to simple inertial oscillation and that the rms deviations in this region should be large. Figure 5 (bottom right) shows, however, that the winds in the three lowest levels have the smallest rms deviations. The amplitude $A(z_i)$ and steady-state alongfront wind u_{ss} decrease below the inversion, but the winds still appear to evolve as a simple inertial oscillation.

Figure 6 shows time series plots of observed and least-squares fit winds for the surface and selected levels of the Seneca profiler. These plots show the overall better fit for the v data (right). At the surface (bottom) the amplitude of inertial oscillation is so small (≈1 m s^{-1})

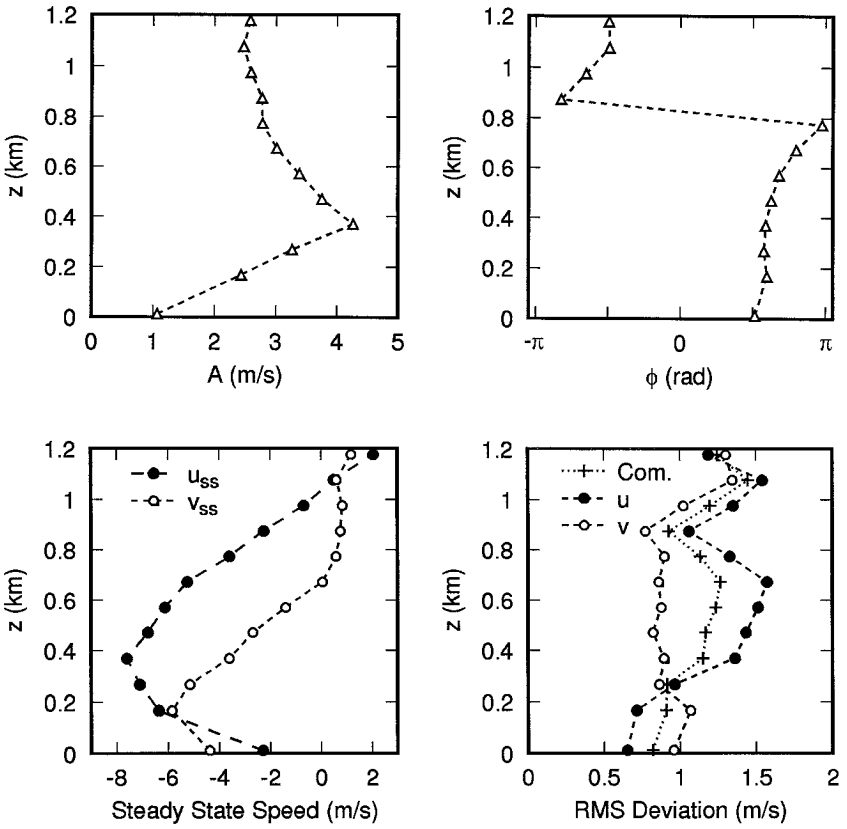

FIG. 5. Results of least-squares fit of Seneca boundary layer profiler and collocated PAM winds to Eq. (1) for an inertial oscillation. Height-dependent amplitude A (top left), phase ϕ (top right), steady-state winds u_{ss} and v_{ss} (bottom left), and root-mean-square deviations, combined and separate for u and v alone (bottom right).

that it is debatable whether it is occurring. If one adopts the arbitrary condition that the amplitude must be at least double the rms deviation in order for inertial oscillation to be clearly indicated, then the surface and the second-highest level are the only ones that fail to show it. All levels exhibit seemingly random higher frequency oscillations about the basic inertial oscillation.

A second boundary layer profiler, at Humboldt, Nebraska, 32 km north-northeast of Seneca, also has a continuous record of wind profiles throughout the night, and these data also show similar characteristics of an inertial oscillation. The same least-squares fit computation with the Humboldt boundary layer profiler and collocated PAM data yield values (not shown) of the parameters (u_{ss}, v_{ss}, A, and ϕ) that agree well with the Seneca values, with two exceptions: the amplitudes of the inertial oscillation in the highest levels are greater, and the shear of u_{ss} is smaller above the jet maximum. Aside from these discrepancies, the agreement with the earlier results is quite good, particularly below $z \approx 1000$ m.

The results of the least-squares fits of boundary layer profiler data to the inertial oscillation solution with linear drag (contained in the appendix) provide no strong evidence that the evolution of the wind is damped. In fact, where this effect is most expected (near the ground), the fit reverts to the undamped solution. It is possible that energy is being supplied to the lower-level winds at just the correct rate to offset the damping. More likely it is the existence of the relatively deep nearly mixed layer instead of a surface inversion that reduces the effect of damping to an unobservable level. If the drag is acting to slow a layer 400 m thick, the impact is much smaller than if it acts on a much shallower layer decoupled from the rest of the boundary layer by a surface inversion.

3. Baroclinic Ekman–Taylor model and steady-state wind profiles

Once the inertial oscillation in the wind data is established and quantified, the task of understanding the other processes that control the u and v wind profiles is simplified. The data suggest, and the following analyses confirm, that this oscillation takes place independently of the physics that is controlling the equilibrium (steady-state) profiles. Predictions of the variation of wind with height based on accepted models that evolve

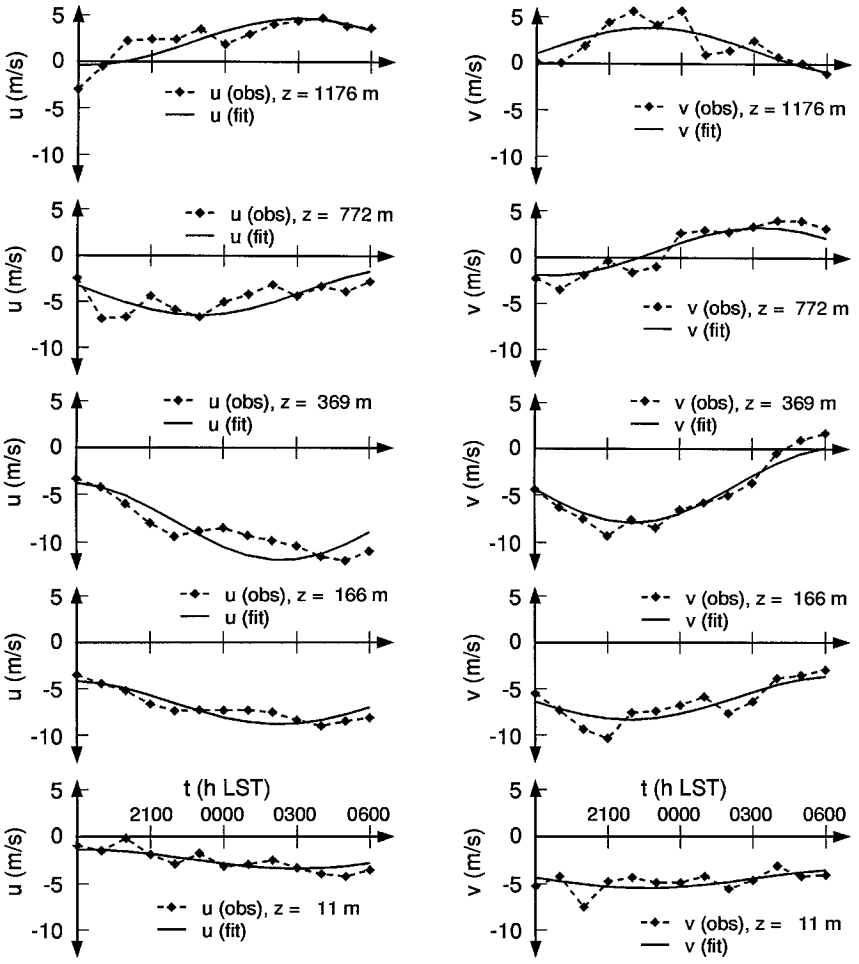

FIG. 6. Plots of observed and least-squares fit u (left) and v (right) vs time. From bottom to top: surface PAM station, lowest level of Seneca boundary layer profiler, level of jet maximum and largest-amplitude inertial oscillation, an intermediate upper level, and highest profiler level used.

slowly with time apply to these steady-state profiles, not to the rapidly changing hourly wind data.

The steady-state profiles for this event can be modeled using two layers that are indicated in the potential temperature profiles as well as in the alongfront jet (Figs. 3 and 4.) The stable layer above 400 m applies to the semigeostrophic frontogenesis model. (This is shown in the next section.) Wind profiles in the nearly neutral layer below the inversion will be examined with a simple baroclinic boundary layer model. This model consists of an Ekman layer with a height-dependent geostrophic wind that is matched to a surface layer. The following is an abbreviated description of the model presented by Bannon and Salem (1995). The horizontal momentum equations for the layer are

$$f\mathbf{k} \times (\mathbf{u} - \mathbf{u}_g) = \kappa \frac{\partial^2 \mathbf{u}}{\partial z^2}, \tag{3}$$

where κ is the constant coefficient of eddy diffusion of momentum and $\mathbf{u}_g$ is the geostrophic wind. The north–south temperature gradient combined with a pervasive nearly neutral temperature profile causes $\mathbf{u}_g$ to vary linearly with height z,

$$\mathbf{u}_g = \mathbf{u}_{g0} + u_{gz} z \mathbf{i}, \tag{4}$$

where $\mathbf{u}_{g0}$ is the geostrophic wind at the surface and u_{gz} is the constant wind shear given by the thermal wind equation

$$u_{gz} = -\frac{g}{f\theta_0}\frac{\partial \theta}{\partial y}. \tag{5}$$

The acceleration of gravity is g and θ_0 is the ambient potential temperature.

The solution of (3) is

$$\mathbf{u} = \mathbf{u}_g + e^{-\eta}[(\mathbf{u}_0 - \mathbf{u}_{g0})\cos\eta - \mathbf{k} \times (\mathbf{u}_0 - \mathbf{u}_{g0})\sin\eta], \tag{6}$$

with $\eta = z/H$, H is the Ekman depth given by

$$H = (2\kappa f^{-1})^{1/2}, \tag{7}$$

and $\mathbf{u}_0$ is the wind at the bottom of the Ekman layer. This level, $z = 0$, corresponds to the top of the surface layer, which has a depth h. The matching condition for the winds in the two layers is the Taylor (1915) condition, which can be written as

$$\frac{\partial \mathbf{u}}{\partial z} = \frac{A}{H}\mathbf{u} \qquad (z = 0), \tag{8}$$

where A is a dimensionless parameter related to the properties of the surface layer. It lies in the range $0 \leq A \leq 10$ (Bannon and Salem 1995), with the higher values corresponding to stable conditions.

The matching condition (8) is satisfied by

$$\mathbf{u}_0 = \frac{(2 + A)\mathbf{u}_{g0} + (1 + A)Hu_{gz}\mathbf{i} + \mathbf{k} \times (A\mathbf{u}_{g0} - Hu_{gz}\mathbf{i})}{[1 + (1 + A)^2]}. \tag{9}$$

The quantities appearing in the expressions for the wind [(6) and (9)] can be grouped into those that can be measured directly or estimated with reasonable accuracy (u_{gz}, h) and those that cannot ($\mathbf{u}_{g0}$, A, H). The observed steady-state winds in the Ekman layer (the three lowest profiler levels) and in the surface layer (the PAM station) are fit to the Ekman–Taylor model by adjusting the values of the latter quantities to minimize the rms deviation between the steady-state winds and the solutions. Surface temperature measurements yield an average value of $u_{gz} = 0.014$ s^{-1} throughout the period of the inertial oscillation. The surface layer depth h is estimated to be 20 m, based on the friction velocity reported by the Atmosphere–Surface Turbulent Exchange Research facility, located a few kilometers from the Seneca profiler. Repeating the calculation for $h =$ 40 m yields essentially the same result.

The least-squares fit was performed as in section 2. A logarithmic wind profile was assumed in the surface layer in order to use the PAM winds to give the steady-state wind at the matching level needed for (9). The results of this fit yield an rms deviation of 0.52 m s^{-1} for the eight wind speeds. The values of the adjusted parameters are $H = 210$ m, $A = 1.9$, and $\mathbf{u}_{g0} = (-11.3, -2.4)$ m s^{-1}. The latter agree rather well with the estimated geostrophic winds (discussed in section 5), considering the uncertainties associated with the latter computation.

The inertial oscillation steady-state wind profiles and the best-fit Ekman–Taylor solution are shown in Fig. 7, along with the model predictions for the winds in the upper layer (discussed in section 4). The plot shows that the Ekman–Taylor model solution is a relatively good fit to the steady-state winds. The most significant departure is in u at the top of the layer, and that difference is only 0.65 m s^{-1}. Given that the height of the boundary between the two layers most likely varied throughout the night, some discrepancy at this height is not unexpected.

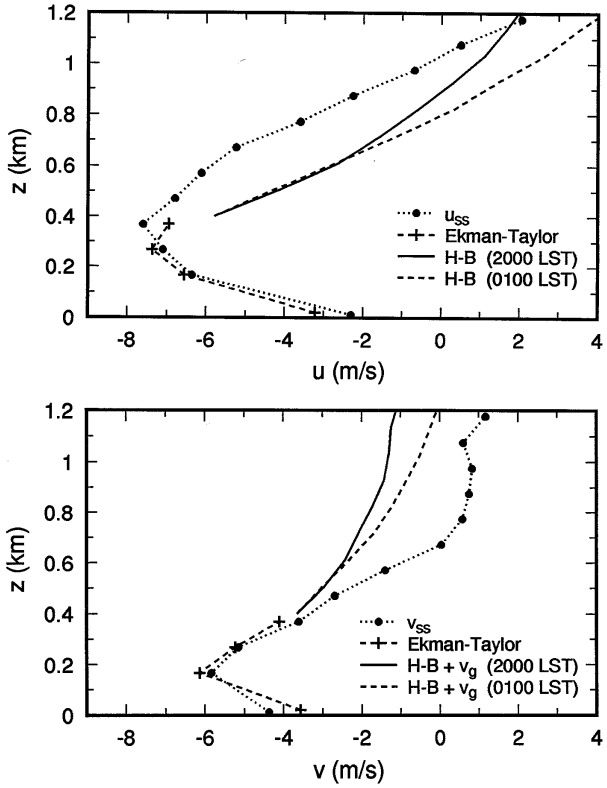

FIG. 7. Profiles of alongfront (top) and cross-front (bottom) winds at Seneca: least-squares fit to Ekman–Taylor model ($z < 0.4$ km), Hoskins–Bretherton (H–B) frontogenesis model predictions ($z > 0.4$ km), and steady state from the least-squares inertial oscillation fit to profiler and PAM data. 2000 LST 20 February 1992 and 0100 LST 21 February 1992 are the beginning and ending times of the period of frontogenesis.

4. Boundary layer influence on the observed frontogenesis

The observed inertial oscillation in the boundary layer during the night of 20–21 February is connected to the frontogenesis that occurs during the first part of the period in a couple of important ways. As was pointed out in OB, the alongfront winds u_g predicted by the semigeostrophic model (Hoskins and Bretherton 1972) differ considerably from the observed winds. The latter change much more rapidly and by a much larger amount (Fig. 4, top) than the predicted winds, the vertical shear of u in the lowest ~400 m is negative while the thermal wind equation requires the geostrophic flow to have positive shear, and the vertical shear in the upper part of the layer is larger than the geostrophic wind shear (OB, Fig. 10, bottom). These discrepancies cast serious doubt on the applicability of the semigeostrophic model to this case because they suggest that the winds are not constrained by thermal wind balance, in direct contradiction to a basic feature of the model. By dividing the region into two layers as described in section 3 and assuming that the observed winds reflect an unbalanced pressure gradient force with a superposed inertial os-

cillation, the disagreement between semigeostrophic theory and observation in the upper layer is resolved. The reversed shear in the lower layer is resolved by the Ekman–Taylor model.

The upper part of Fig. 7 shows three plots of alongfront winds: u_g predicted by the Hoskins–Bretherton model for 2000 LST 20 February 1992, when the frontogenesis began; the model prediction 5 h later at the end of the period of frontogenesis; and u_{ss} from the least-squares inertial oscillation fit (Fig. 5, bottom left). Each predicted u_g profile is the analytical solution for u_g from the Hoskins–Bretherton model (OB, section 5c) to which is added a uniform zonal wind, so that the sum at the lower boundary matches the geostrophic wind at the top of the Ekman–Taylor layer [the **i** component of (4)].

The changes in the zonal wind speeds and wind shear during the night (see Fig. 4, top) are much greater than those predicted by the Hoskins–Bretherton model. This is because the height-dependent inertial oscillation is causing much larger and more rapid changes in the wind speeds, profile shape, and size of vertical wind shear than those produced by deformation frontogenesis. The changes caused by inertial oscillation can, to a good approximation, be subtracted out of the observed winds by comparing the predicted profiles to the steady-state alongfront wind u_{ss} from the least-squares fit, rather than to the individual hourly profiles. The vertical shear in u_g at 0100 LST agrees quite well with that of u_{ss}. Since there is a nearly mixed layer, the same horizontal temperature gradient shown in surface data exists several hundred meters above the ground. Consequently the thermal-wind-generated shear predicted near the ground by this inviscid model is displaced upward to above the top of the Ekman–Taylor layer. Alongfront thermal wind balance, a key component of the semigeostrophic frontogenesis model, does apply in the upper layer.

While this interpretation of the events controlling the alongfront winds aloft resolves some major conflicts between observations and predictions, the picture is still incomplete. The assumption that the ageostrophic zonal wind goes to zero abruptly at the boundary between the two layers results in a jump in u. This may be due to changes in the height of the inversion (and therefore the boundary between the two layers) throughout the night. The predicted steepening of the vertical shear (on the order of 0.003 s^{-1}) during the frontogenesis cannot be tested using the simple inertial oscillation fit. It is so small that it is doubtful that any technique could detect it unambiguously given the noise in the wind data. While the profile of u_{ss} above ~400 m is in fairly good agreement with the predictions, it shows an increase in vertical shear above ~700 m, where a reduction would be expected based on the model solution profiles. This may also be related to the height of the inversion decreasing throughout the night. The largest rms difference in the inertial oscillation fit (Fig. 5, bottom right) is in the 400–700 m region. While the agreement between the predicted profiles and u_{ss} above 400 m is not perfect, it is far better than is found when the hourly averaged winds are used.

Larger than predicted alongfront wind shears that also appear in the 0500 LST soundings (Fig. 3, middle) are likely due to inertial oscillation as well. Since multiple soundings were not taken throughout the night at these sites, it is not possible to apply the analysis that was used to detect inertial oscillation in the profiler data. Consequently, there is no direct evidence that the evolution of the winds during the 12 hours prior to these soundings was controlled by simple inertial oscillation.

The available upper-air wind data provide convincing, though incomplete, evidence that i) inertial oscillation controls the rapid changes in winds in the lowest ~1 km of the atmosphere during the frontogenesis, and ii) the thermal wind relation in the semigeostrophic model establishes the vertical shear in the steady-state alongfront wind u_{ss} above the weakly stable layer.

A related consideration is the profile of the cross-front wind v in the upper (stable) layer. The ageostrophic part of the cross-front wind v_a, derived by Davies and Müller (1988) from the diagnostic equation [OB, (19)] for the cross-front circulation, is given by

$$v_a = \frac{\alpha}{f}\left(u_g + z\frac{\partial u_g}{\partial z}\right), \tag{10}$$

where α is the measured deformation parameter (2×10^{-5} s^{-1}) and u_g is the zonal geostrophic flow solution displayed in Fig. 7 (top). The uniform geostrophic wind v_g found in the Ekman–Taylor analysis (section 3) is added to v_a to get the total cross-front wind in the frontogenesis layer. Figure 7 (bottom) shows these predicted profiles at the beginning and at the end of the period of frontogenesis, together with v_{ss} from the least-squares inertial oscillation fit (Fig. 5, bottom left). The solutions for v in the two layers are in rather good agreement at their boundary ($z = 400$ m), but the shear in v_{ss} between 400 and 700 m is considerably greater than predicted. Why does the semigeostrophic model seem to fail at predicting the observed magnitude of the shear in v_a even after the inertial oscillation is removed from the v observations? This is the same height range that is problematic in the u profiles, so it may be related to changes in the depth of the nearly mixed layer. But another important factor may be the sloping terrain around Seneca.

The large shear in v_{ss} between 400 and 700 m suggests the existence of a significant east–west temperature gradient. The surface data do not indicate any gradient during the period, but there can be a gradient aloft caused by the combination of increasing potential temperature above the nearly mixed layer and the gradual incline of the ground from east to west. In particular,

$$\frac{\partial \theta}{\partial x} \approx \frac{\partial \theta}{\partial z}\left(-\frac{\partial z_{gr}}{\partial x}\right), \tag{11}$$

where $\partial z_{gr}/\partial x$ is the east–west slope of the ground. This would produce a thermal wind given by

$$\frac{\partial v}{\partial z} = \frac{g}{f\theta_0}\frac{\partial \theta}{\partial x} \approx -\frac{g}{f\theta_0}\frac{\partial \theta}{\partial z}\frac{\partial z_{gr}}{\partial x}. \quad (12)$$

Rough estimates of this shear in v can be made using the Topeka 0500 LST 21 February sounding (Fig. 2, top) and elevation data for the area. The former shows $\partial\theta/\partial z \approx 0.045$ K m^{-1} at $z = 500$ m. A linear least-squares fit of elevation versus longitude for 10 surface stations within 50 km of Seneca yields -0.88 ± 0.41 m km^{-1} as an estimate of $\partial z_{gr}/\partial x$. The resulting shear in v is ≈ 0.015 s^{-1}, which is actually larger than $\partial v_{ss}/\partial z$ at 500 m (Fig. 7, bottom). The Topeka sounding shows a reduction in $\partial\theta/\partial z$ above 600 m, which may account for the greatly reduced shear in v_{ss} in that region.

There are a number of factors that cause large uncertainties in this analysis. It assumes that the potential temperature profile is constant throughout the period and that it does not vary with x. The former assumption cannot be tested and is unlikely to be true. The uncertainties in $\partial z_{gr}/\partial x$ are large as well, since it is not clear what horizontal scale should be used in computing the ground slopes. However, this simple calculation does show that the sloping terrain could contribute a shear in v that has both the proper sign and correct order of magnitude to account for the discrepancy between the shears in v_a and v_{ss} above the nearly mixed layer.

The elevation data do not show a significant north–south slope around Seneca (the correlation between elevation and y is -0.34), so it is not likely that the terrain affects the shear in u_{ss}.

5. Surface inertial oscillation and the rate of frontogenesis

The accelerating geostrophic winds throughout much of the frontal region during the night of 20–21 February 1992 apparently contributed to a rare phenomenon: evidence of inertial oscillation in surface wind data (10-m level). Pressure data from across Iowa, Illinois, and eastern Missouri yield geostrophic winds that are changing in speed, turning clockwise, or both, precisely the type of forcing that enhances inertial oscillation. This may also affect the rate of frontogenesis.

During the night of 20–21 February 1992, the geostrophic wind was likely to be changing because of eastward movement of the deformation flow field and, for part of the period, frontogenesis. The geostrophic wind in the vicinity of the Seneca boundary layer profiler was computed using hourly averaged pressure data taken at 12 surface stations in a 200 km by 200 km area. (A smaller region would be more desirable in order to minimize the effects of nonuniform pressure gradient, but the standard errors in the calculations of the geostrophic wind using only the nearby PAM stations are unacceptably large.) A linear least-squares fit of the altitude-corrected pressure data versus y and versus x yields the

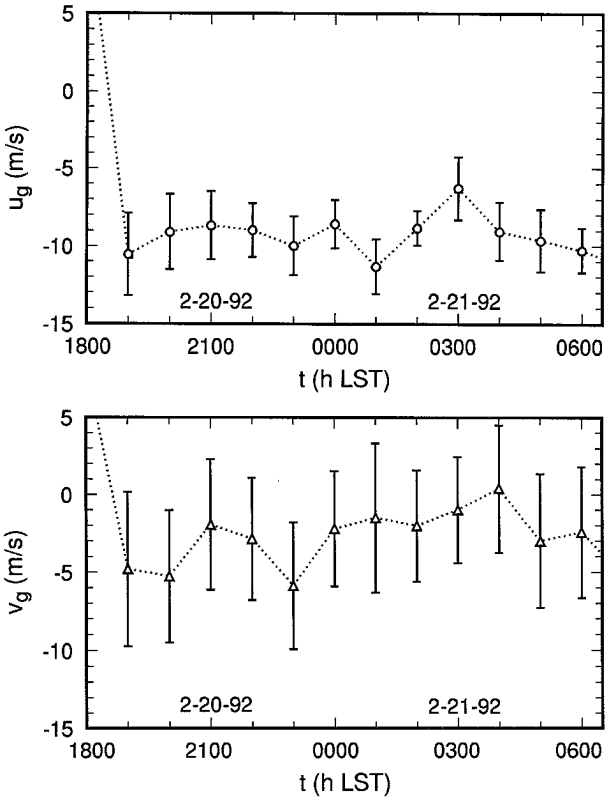

FIG. 8. Geostrophic winds at Seneca during the night of 20–21 February 1992. The values include standard errors computed from the linear regression of pressure data from 12 nearby surface stations.

values plotted in Fig. 8. Even though data from 12 stations were used, the uncertainties in the geostrophic wind, particularly v_g, are quite large. The westerly component u_g remains close to 10 m s^{-1} throughout most of the period, while v_g shows a net increase from 1900 to 0400 LST.

Least-squares fit of wind data from 85 surface stations to an inertial oscillation was also carried out. The computed parameters for 24 selected stations satisfy two criteria for the existence of this oscillation: the amplitude is both greater than 2 m s^{-1} and at least twice the rms deviation. The locations of these stations are marked with a "⊕" in Fig. 1. Several of the stations are on the warm side of the front during the night. An additional 14 sites (not shown) pass the second criterion for the establishment of an inertial oscillation but have amplitudes less than 2 m s^{-1}.

Two examples of an inertial oscillation in surface wind data are shown in Fig. 9. PAM 4, north of the front, is located near the Iowa–Missouri border, and PAM 25 is 370 km to the southwest, on the other side of the front. The amplitudes of the inertial oscillation and the rms deviations are 2.3 m s^{-1} and 0.75 m s^{-1}, respectively, for PAM 4, and 2.5 m s^{-1} and 1.1 m s^{-1}, respectively, for PAM 25.

The two plots of meridional wind in Fig. 9 suggest

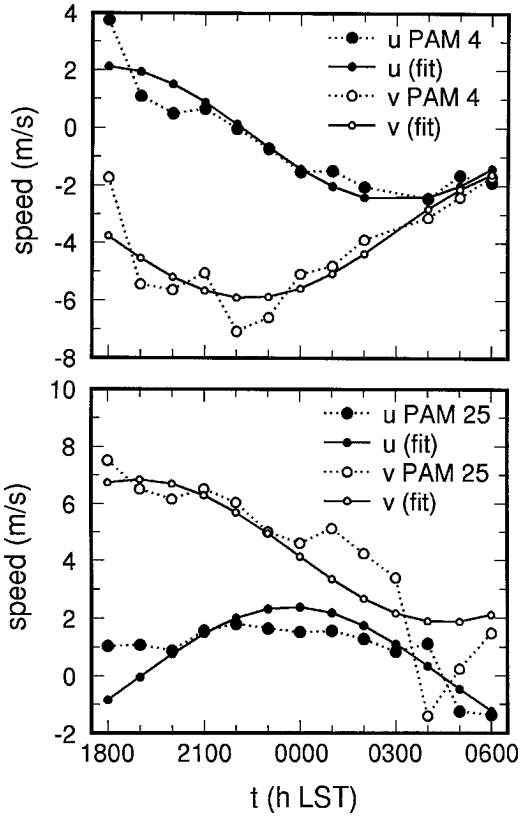

FIG. 9. The inertial oscillation recorded by the surface stations PAM 4 (upper) and PAM 25 (lower) between 1800 LST 20 February and 0600 LST 21 February.

a means by which frontogenesis and an inertial oscillation may be coupled: the latter causes changes in the confluent north–south wind that produces, and therefore controls the rate of, frontogenesis. There is only circumstantial evidence to support this hypothesis because only a minority of surface stations show inertial oscillations taking place. However, Fig. 9 and OB Fig. 5 show that the strongest confluence (maximum $|v_y|$) occurs at about the same time (2200 LST) that the inertial oscillation produces the maximum $|\Delta v|$ between these two sites.

It is instructive to reconsider the analysis of OB (section 4a) in light of the current discussion. Of the 62 surface stations used to calculate the deformation parameter α (OB Fig. 5) and the potential temperature gradient (OB Fig. 6), 12 exhibit an inertial oscillation. There is a strong negative correlation (-0.94) between the y position of these stations and the steady-state southerly wind speed v_{ss}. The slope $(v_{ss})_y$ of the linear regression for these quantities is -0.021 m s^{-1} km^{-1}, very close to the average value of v_y. Eight of these stations are north of the front and have $v_{ss} < 0$. The data from seven of these show maximum northerly wind speed occurring between 2100 and 2300 LST. This suggests that the variation of v_y with time seen in OB Fig. 5 may be caused by the presence of inertial oscillations. But this cannot be proven conclusively since wind data from most of the surface stations do not meet the two criteria for the existence of inertial oscillations.

Given the large amplitude inertial oscillations seen in the boundary layer profiler data, it is easy to speculate that the rate of frontogenesis higher up in the boundary layer may have been very strongly influenced by the oscillations. Estimates of v_y using only the Seneca and Humboldt profilers are unreliable given their close proximity. The absence of supplemental soundings from sites spread across the region, or any other source of winds aloft data in the lowest few hundreds of meters, makes it unlikely that this possibility can be verified.

6. A related example and additional remarks

A key piece of information that is lacking about this event is the evolution of the thermal profile of the boundary layer. The intermediate steps in the transition from the deep, daytime convective mixed layer shown in the evening soundings (Fig. 2) to the shallower, nearly neutral layer in the following morning soundings (Fig. 3) are unknown. The success of the two-layer model presented in sections 3 and 4 suggests that the height of the boundary between the two layers was established early during the night and remained roughly constant. Conclusive proof is, however, absent.

A similar event took place nine days earlier, during an intensive observation period. Supplemental soundings were taken every 3 h throughout the night, providing a much clearer picture of how the boundary layer evolved. Figure 10 displays the soundings taken at Omaha during the night of 11–12 February 1992. Although the cold air advection is weaker than on the night of 20–21 February, the easterly low-level jet and the shallow, nearly mixed layer in the 0500 LST sounding are very similar. The temperature profiles indicate that the depth and stability of this layer changed very little after 2000 LST.

Another important similarity between these two events is evidence for an inertial oscillation. Analysis reveals that the large changes in winds at the 800-m level fit the criteria for the inertial oscillation (the amplitude is 3.8 m s^{-1} and the rms deviation is 1.0 m s^{-1}). At all other levels, the amplitudes are less than 2 m s^{-1}. This is an important result because it it shows that the combination of a nearly mixed layer, a low-level jet, and an inertial oscillation on the night of 20–21 February 1992 was not unique.

In summary, this investigation shows that the frontogenesis in the ~1 km thick boundary layer occurred at a time when the temperature profile defined two distinct layers. The nearly neutral lower layer is coupled to the surface by shear-induced turbulence, and its steady-state wind profiles agree with that of a baroclinic Ekman–Taylor model. The wind profiles predicted by the inviscid Hoskins–Bretherton semigeostrophic model are in reasonably good agreement with the observed

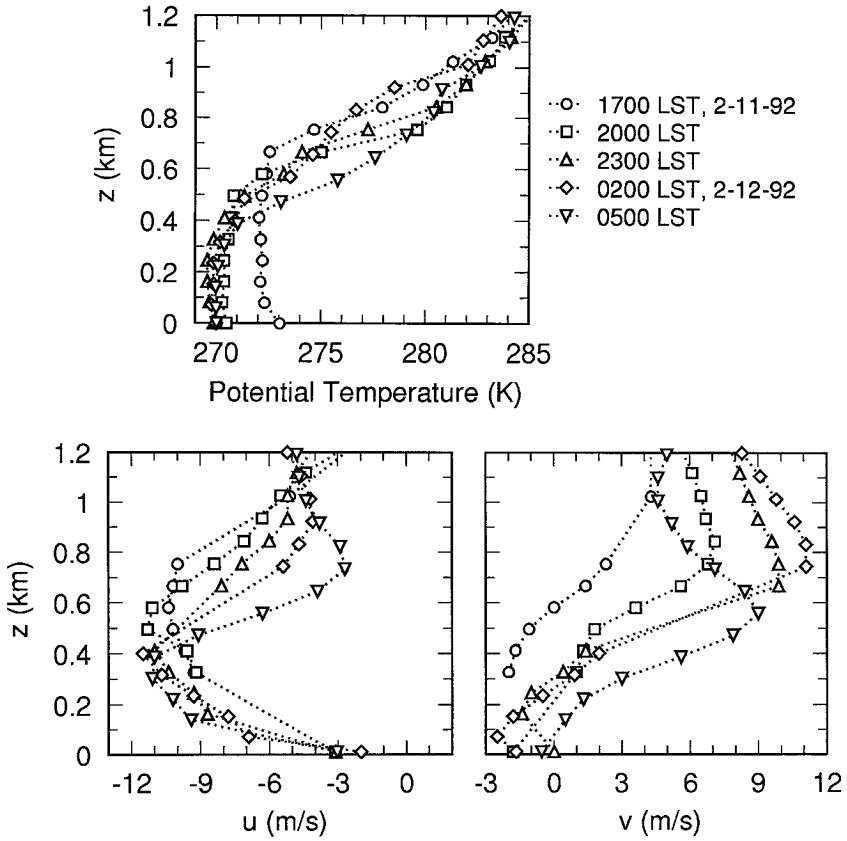

FIG. 10. Vertical profiles of potential temperature, zonal wind *u*, and meridional wind *v*, taken from Omaha soundings and collocated surface station data from the night of 11–12 February 1992.

steady-state profiles in the upper layer. This is revealed only after the height-dependent inertial oscillations in both layers have been filtered out. Left unanswered is the question of how inertial oscillation can take place simultaneously in two layers controlled by such different physical processes. The actual evolution of these two layers remains a mystery because of the lack of temperature data beyond the usual soundings. Such data would likely help explain, for example, the imperfect match in the alongfront winds of the two models at the boundary between the two layers.

A related question is concerned with the effect of inertial oscillations on the frontogenesis itself, particularly at low levels. The principal features that need to be examined are the modifications to the rate of frontogenesis and to the cross-front ageostrophic circulation. There are two features omitted in the balanced models of frontogenesis: one is the effect of boundary layer turbulent stress, while the other is the modification required to include the contribution of unbalanced motions in both the along- and cross-front directions. The present results show that it may be permissible to treat the latter but to neglect the former, at least in situations similar to the frontogenesis event studied here. A modification to the Hoskins and Bretherton (1972) frontogenesis model incorporating this simplification has been considered recently by Blumen (1996).

Acknowledgments. Support for this investigation was provided by the National Science Foundation under Grants ATM-9100171 and ATM-9303111 and by the Air Force Office of Scientific Research under Grants F49620-93-1-0416 and F49620-95-1-0141.

APPENDIX

Test for Damped Inertial Oscillations

Since the lower 300–400 m of the boundary layer during the night of 20–21 February are more or less well mixed, it would not be expected to be decoupled from the surface layer: it should be affected by surface drag. It is therefore reasonable to expect evidence of damping in the wind oscillation. The solution for the winds in the lower layer of the slab model with linear drag, essentially that of Thorpe and Guymer (1977), was used as the basis for a second least-squares fit of the Seneca boundary layer profiler and PAM wind data. These data, u_{ij} and v_{ij}, were assumed to evolve according to the equations

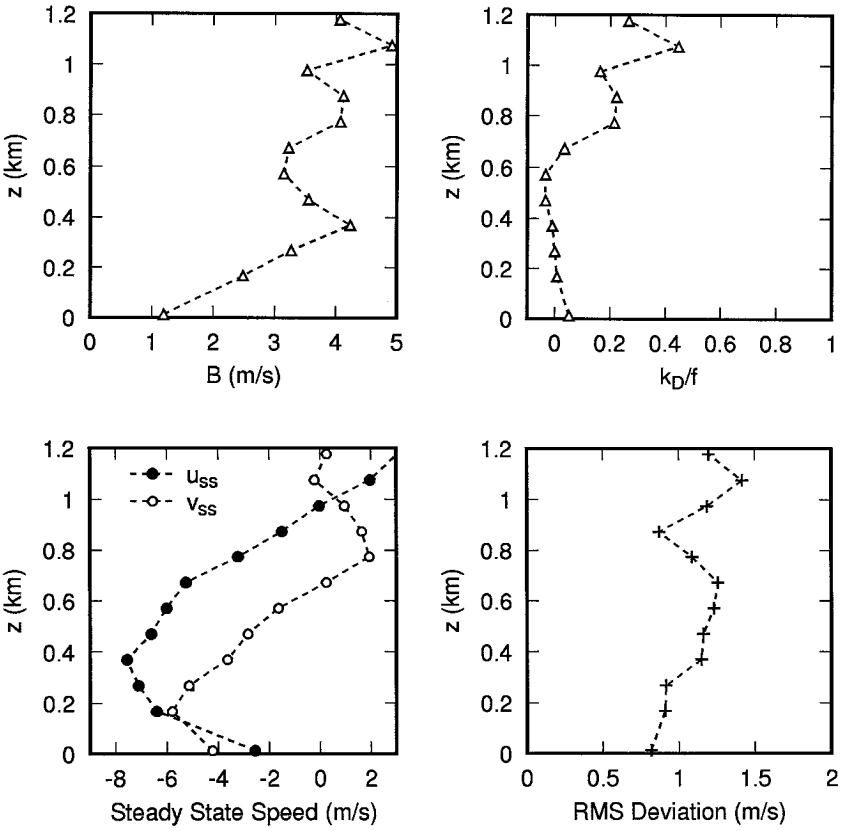

FIG. A1. Results of least-squares fit of Seneca boundary layer profiler and collocated PAM winds to an inertial oscillation with linear drag. Height-dependent initial amplitude B (top left), drag coefficient k_D normalized to f (top right), steady-state winds u_{ss} and v_{ss} (bottom left), and combined root-mean-square deviation (bottom right).

$$u(z_i, t_j) = C_f[\, f u_{ss}(z_i) - k_D(z_i) v_{ss}(z_i)] + B(z_i) e^{-\kappa_D(z_i)t_j} \sin[\, f t_j + \beta(z_i)],$$

$$v(z_i, t_j) = C_f[\, f v_{ss}(z_i) + k_D(z_i) u_{ss}(z_i)] + B(z_i) e^{-\kappa_D(z_i)t_j} \cos[\, f t_j + \beta(z_i)], \quad \text{(A1)}$$

where $C_f = f(f^2 + k_D^2)^{-1}$, $B^2 = [u_d - C_f(f u_g - k_D v_g)]^2 + [v_d - C_f(f v_g + k_D u_g)]^2$, $\tan(\beta) = [u_g - C_f(f u_g - k_D v_g)][(v_g - C_f(f v_g + k_D u_g)]^{-1}$, (u_d, v_d) represent the wind components at $t = 0$ (sunset), k_d is a height-dependent drag coefficient, and (u_{ss}, v_{ss}) are defined in (1). The five height-dependent parameters (u_{ss}, v_{ss}, B, β, and k_D) were adjusted to minimize the combined rms deviation (2). Note that the undamped solution (1) is recovered when $k_D(z_i) = 0$.

The results of the least-squares fit computation are shown in Fig. A1. The drag coefficient $k_D(z)$ (top right) that yields the best fit is essentially zero below 700 m and remains small compared to f at all heights. Compared to the fit for undamped inertial oscillation (Fig. 5), the corresponding parameters for the damped fit are essentially identical below 700 m. Above this level, the initial amplitude B is larger than the undamped amplitude A. This increase is caused by the small changes ($\sim$1 m s^{-1}) in u_{ss} and v_{ss} at these levels. The phase β (not shown) is nearly identical to ϕ in the undamped case, the largest difference being 0.28 radians at $z =$ 1076 m. Below 800 m, the difference between β and ϕ is less than 0.1 rad.

The most telling feature in the comparison between the damped and undamped fits is that the combined rms deviations (Fig. A1, bottom right, and Fig. 5, bottom right) are virtually identical. This is true even in the upper levels where the previously noted differences between corresponding fit parameters are largest. In the lower half of the region being considered, the least-squares fit essentially converges to undamped inertial oscillation. In the upper half the damping is found to be finite, but the fit is no better than with no damping.

The same least-squares fit was performed with the Humboldt boundary layer profiler and PAM data. The results (not shown) show a somewhat greater departure from the undamped fit than did the previous case using Seneca data. Above 700 m, $|k_D|$ is greater than 0.3, and the values of u_{ss}, v_{ss}, and B at these levels depart noticeably from their corresponding values in the undamped case. The initial amplitudes B at the highest two levels are more than double the corresponding values

of *A.* As with the Seneca data, the differences below 700 m are minimal. At all levels below 1000 m, the combined rms deviations are virtually identical to those computed in the undamped case. The damped solution is no better at modeling the evolution of the low-level jet than the undamped solution.

REFERENCES

Bannon, P. R., and T. L. Salem Jr., 1995: Aspects of the baroclinic boundary layer. *J. Atmos. Sci.,* **52,** 574–596.

Blumen, W., 1997: A model of inertial oscillations with deformation frontogenesis. *J. Atmos. Sci.,* in press.

Davies, H. C., and J. C. Müller, 1988: Detailed description of deformation-induced semi-geostrophic frontogenesis. *Quart. J. Roy. Meteor. Soc.,* **114,** 1201–1219.

Hoskins, B. J., and F. P. Bretherton, 1972: Atmospheric frontogenesis models: Mathematical formulation and solution. *J. Atmos. Sci.,* **29,** 11–37.

Kotroni, V., Y. Lemaître, and M. Petitdidier, 1994: Dynamics of a low-level jet observed during the Fronts 87 experiment. *Quart. J. Roy. Meteor. Soc.,* **120,** 277–303.

Ostdiek, V., and W. Blumen, 1995: Deformation frontogenesis: Observation and theory. *J. Atmos. Sci.,* **52,** 1488–1500.

Taylor, G. I., 1915: Eddy motion in the atmosphere. *Philos. Trans. Roy. Soc. London,* **A215,** 1–26.

Thorpe, A. J., and T. H. Guymer, 1977: The nocturnal jet. *Quart. J. Roy. Meteor. Soc.,* **103,** 633–653.